



Voltage relaxation and Abrikosov–Josephson vortices in Bi-2223 superconductors doped with α -Al₂O₃ nanoparticles

M. Hernández-Wolpez¹ · J. R. Fernández-Gamboa² · I. García-Fornaris³ · E. Govea-Alcaide⁴ · E. Pérez-Tijerina⁵ · R. F. Jardim⁶ · P. Muné² 

Received: 16 November 2017 / Accepted: 6 January 2018 / Published online: 13 January 2018
© Springer Science+Business Media, LLC, part of Springer Nature 2018

Abstract

We have observed a change in the behaviour of voltage-relaxation curves with remnant magnetic flux, when the maximum magnetic field applied before starting the relaxation process, H_{am} , reaches 80 Oe in two samples of Bi_{1.65}Pb_{0.35}Sr₂Ca₂Cu₃O_{10+ δ} (Bi-2223) doped with α -Al₂O₃ nanoparticles. This modification consists in the emergence of a maximum in the temporal dependence of the voltage, $V(t)$, which appears in the vicinity of the first 5 s after applying to the sample an excitation current lightly higher than the superconducting critical current of the material. In addition to that, the voltage drop rate increases appreciably with increasing applied magnetic fields. As complementary studies, X-ray diffraction patterns, scanning electron microscopy, measurements of magnetization as a function of applied magnetic field and critical current density are also included. The experimental results corroborate the occurrence of intragranular Abrikosov–Josephson vortices in Bi-2223 ceramic superconductors. Furthermore, the analysis provides a new procedure for detecting penetration of the magnetic flux into intragranular planar defects and clean regions of the grains (crystallites), with increasing applied maximum magnetic field, H_{am} .

1 Introduction

The study of the granularity in Bi-2223 superconductors continue to be a current subject in the Materials Science, due to the fact that they are promising candidates for reducing energy consumption in practical applications, such as magnets, motors, current leads, power cables [1–4] and fault current limiters [5, 6]. The grains in Bi-2223 superconductors

have a complex structure due to their high intrinsic anisotropy [7] and a network of planar defects [8]. These defects, such as stacking faults [9] or colonies of low angle boundaries, greatly affect the determination of the lower critical field of the grains, H_{c1g} , that is commonly defined as the magnetic field starting from which the magnetic flux penetrates into the grains.

In a previous paper Hernández-Wolpez et al. [10] have demonstrated that in the interval of applied magnetic fields, H_a , between 30 and 80 Oe, the penetration and trapping of the magnetic flux occur through intragranular defects which are assumed to be planar defects are described above.

More recently, it has been shown that the magnetic flux penetrates into planar defects as Abrikosov–Josephson (AJ) vortices [11] taking into account the values of applied magnetic field at which the phenomenon is observed [12]. In that paper, they first showed that the intrinsic anisotropy of the grains may be compensated by their shape anisotropy. Afterwards, by using a brief theoretical formulation, they estimated the minimum misorientation angle of the intragranular planar defects where the AJ vortices emerge for a given applied magnetic field was estimated. Finally, they found the planar defect angles that correspond to lower critical fields reported for whiskers [13] and textured ceramics

✉ P. Muné
mune@uo.edu.cu

¹ Departamento de Física, Universidad de Camagüey, Ctra. Circunvalación Norte, Km 5 1/2, Camagüey, Cuba

² Departamento de Física, Universidad de Oriente, Patricio Lumumba s/n, P. O. Box 90500, Santiago de Cuba, Cuba

³ Departamento de Ciencias Básicas, Universidad de Granma, Apdo. 21, P.O. Box 85100, Bayamo, Cuba

⁴ Departamento de Física, Universidade Federal do Amazonas, Av. General Rodrigo Octávio, 6200 Coroado I, Manaus 69077-000, Brazil

⁵ Centro de Investigación en Ciencias Físico-Matemáticas, FCFM, UANL, Monterrey, Nuevo León, Mexico

⁶ Instituto de Física, Universidade de São Paulo, CP 66318, São Paulo, SP 05315-970, Brazil

[14] which are related with the two main direction of the grains. These experiments and calculations allow evaluating the intragranular structure of defects in powder and pellet samples of Bi-2223 superconductors.

On the other hand, Altshuler et al. [15] have reported voltage relaxation measurements in polycrystalline $\text{YBa}_2\text{Cu}_3\text{O}_{7-\delta}$ samples. They assumed the voltage, which was detected by the classical four probe method, as indirect measurement of intragranular magnetization. For trapped fluxes in samples subjected to applied magnetic fields below the lower critical field of the grains, the voltage relaxation was absent. The authors then concluded that in their samples there was not trapped flux along the intergranular region inside the detection limits of the measuring system [15]. However, the study of the voltage-relaxation with remnant magnetic flux in form of AJ vortices inside these superconducting materials have not been reported yet, as far as the authors know.

In order to improve the electric transport properties of the Bi-2223 superconducting samples, the doping with nanoparticles (NPs) have been used for several authors [16–19]. In two of these works, alumina NPs in a Bi-2223 matrix were introduced [16, 17]. However, the authors did not study the voltage relaxation curves in those samples.

In this work, we have observed a different behaviour in the voltage-relaxation curves with remnant magnetic flux, when the maximum applied magnetic field before starting the relaxation process, H_{am} , reaches 80 Oe. This difference consists in the emergence of a maximum in the temporal dependence of the voltage, $V(t)$, which appears close $t = 5$ s after applying an excitation current lightly higher than the critical one at 77 K. The phenomenon is studied in polycrystalline Bi-2223 samples doped with $\alpha\text{-Al}_2\text{O}_3$ NPs. The results are explained assuming the presence of Abrikosov (A) and AJ vortices within the material. Also, the results add new experimental findings regarding the detection of AJ vortices in Bi-2223 granular superconductors. In summary, we are offering a new procedure to detect the penetration of the magnetic flux in polycrystalline sample of Bi-2223: first into the intragranular planar defects; and then into the free of defects regions of the grains or crystallites, when increasing values of $0 < H_{am} \leq H_{c1g}$ are applied.

2 Experimental details

The samples used in this study were prepared from powders of Bi_2O_3 , PbO , SrCO_3 , CaCO_3 , and CuO , which were mixed in an atomic ratio of Bi:Pb:Sr:Ca:Cu (1.65:0.35:2:2:3) to obtain samples with nominal composition $\text{Bi}_{1.65}\text{Pb}_{0.35}\text{Sr}_2\text{Ca}_2\text{Cu}_3\text{O}_{10+\delta}$. Details of the samples preparation process are described elsewhere [20]. Before the last heat treatment, the powders were mixed with different

contents of $\alpha\text{-Al}_2\text{O}_3$ NPs (diameter ~ 40 nm): 0.3 wt% (B03) and 0.5 wt% (B05) samples of the total masses using isopropanol to avoid the NPs agglomerations. These samples were uniaxially compacted at 249 MPa after adding $\alpha\text{-Al}_2\text{O}_3$ NPs and heat-treated in air, at 845 °C for 12 h.

The phase purity of the samples was investigated by X-ray diffraction patterns (XRD) using $\text{Cu K}\alpha$ radiation. Powder diffraction patterns were collected at room temperature with a Bruker D8 advanced diffractometer by using the scanning mode with a step size $\Delta(2\theta) = 0.02^\circ$ and $3^\circ < 2\theta < 80^\circ$ during 3 s of counting time.

The study of the morphology of the samples was done by using scanning electron microscopy (SEM). The average grain's size of both pellet and powder samples also was determined by the same technique with the help of NOVA nano SEM 200 microscope operating between 10 and 15 kV.

In all the cases from the same ceramic superconductors, two types of samples were extracted: pellet and powder for measurements of flux-trapping and voltage relaxation curves, and $M(H_a)$, respectively. A piece of the pellet was manually milled during 15 min to obtain the powder samples. Magnetization as a function of low applied magnetic fields, $M(H_a)$, were measured by using a commercial Quantum Design SQUID magnetometer. In these experiments, powders of a given sample were cooled in zero applied magnetic field from room temperature down to 77 K. After this step, the applied magnetic field, H_a , was then increased from 0 to 500 Oe, in steps of 5 Oe and the magnetization was measured for each value of H_a .

Measurements of $J_c(0, H_{am})$ were performed using the standard dc four-probe method in pellet samples with typical dimensions of $d = 0.5$ mm (thickness), $w = 2$ mm (width), and $l = 10$ mm (length). This type of measurement corresponds to the so-called *flux-trapping curves*, as described elsewhere [21]. The samples are cooled down to 77 K in zero applied magnetic field, similarly to the described above. Then, a certain value of maximum applied magnetic field, H_{am} , is applied to the sample for approximately 30 s, reduced to zero, and the critical current density is determined from the I versus V curve by using the criterion of 1 μV . Finally, the sample is warmed up to temperatures higher than the superconducting critical temperature and cooled down to 77 K in zero applied magnetic field. By repeating these steps for different values of H_{am} , the *flux-trapping curve* is obtained.

Measurements of voltage relaxation $V(t)$ were performed in similar way as described elsewhere [15]. The first steps are the same described for the measurements of $J_c(0, H_{am})$ until the application of the H_{am} and its reduction to zero. After this step, an excitation current lightly higher to the critical one of the material is applied and then the voltages and the corresponding intervals of time are automatically registered.

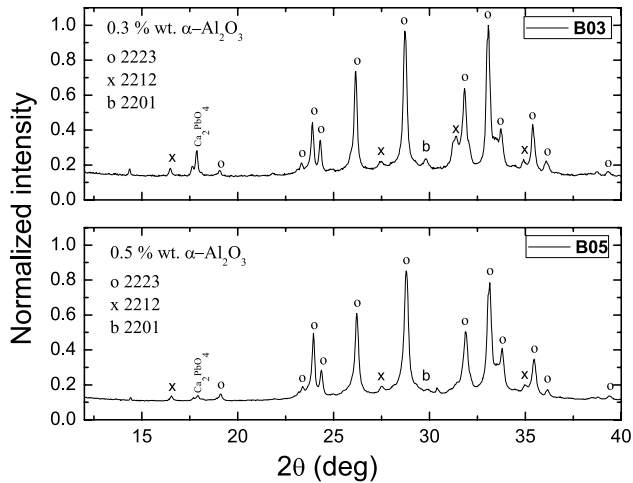


Fig. 1 XRD patterns of the B03 and B05 samples

3 Results and discussion

3.1 Microstructural characterizations

The studied samples are composed by a mixture of phases in which the Bi-2223 phase coexists with others, such as: Bi-2212, Bi-2201 and Ca_2PbO_4 . The determination of the phase composition was performed by using a similar method to that reported in Refs. [22, 23]. The volume fraction of the Bi-2223 phase was found to be ~85%; a similar fraction to that reported elsewhere [10]. The main important result from XRD patterns focused in the objective of this article, is that there are no changes in the XRD peak positions similar to another work [17]. This result explains the fact that the stoichiometry of the grains of the Bi-2223 phase is not modified by doping with $\alpha\text{-Al}_2\text{O}_3$ NPs (Fig. 1).

In Fig. 2 the platelet-like shape of the grains [17, 24] of the samples is displayed. Notice that, different doping percentages do not provoke great modifications in the granular morphology of the ceramics judging by the mean grain's size, which is the similar for the two samples in pellet, but different in the powder samples. Probably the increase of

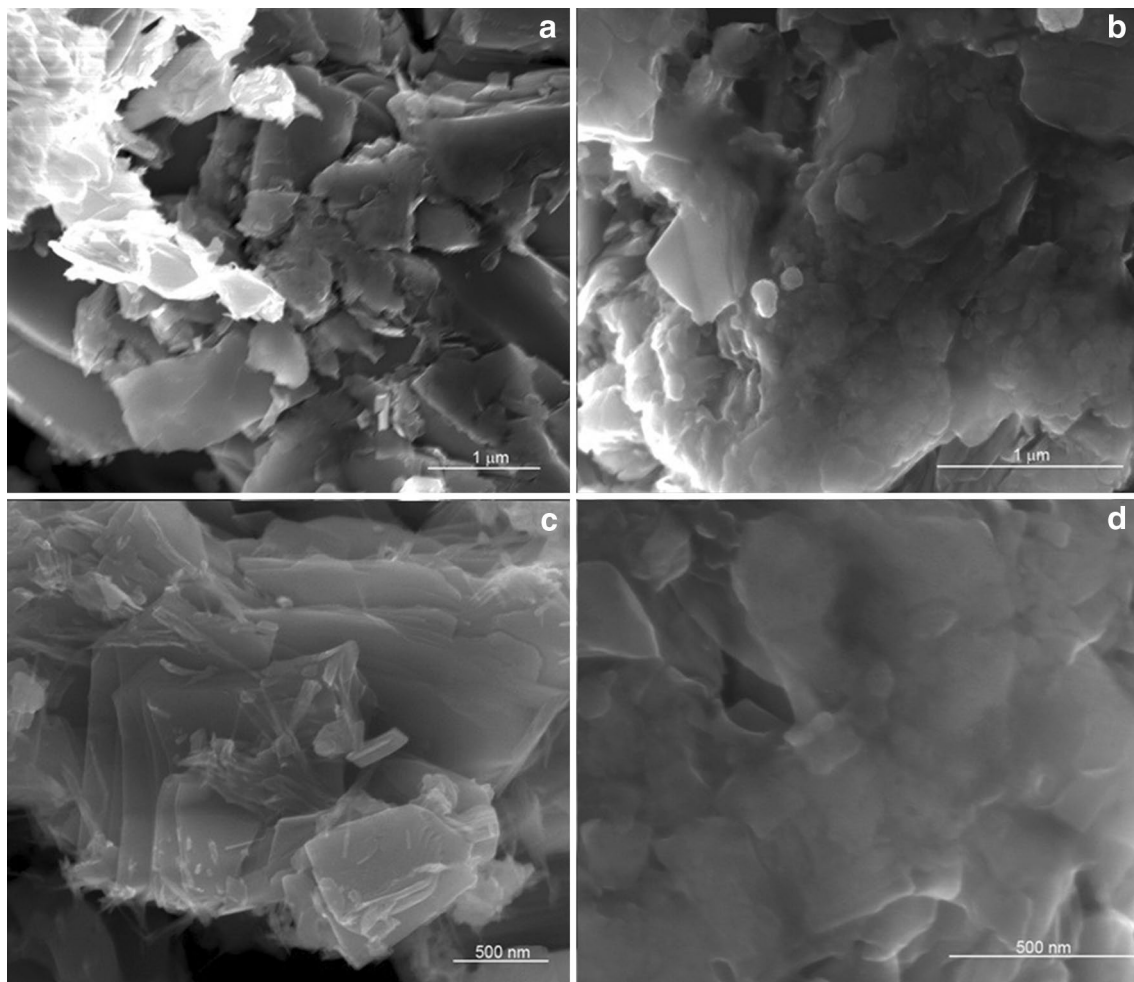


Fig. 2 SEM micrographs of the pellets and powder samples, respectively: B03 (a, c) and B05 (b, d)

Table 1 Grain's size of the samples set

Samples	L_a (μm)	L_c (μm)
B03 powder	0.8	0.04
B03 pellet	0.7	0.09
B05 powder	0.4	0.01
B05 pellet	1.00	0.1

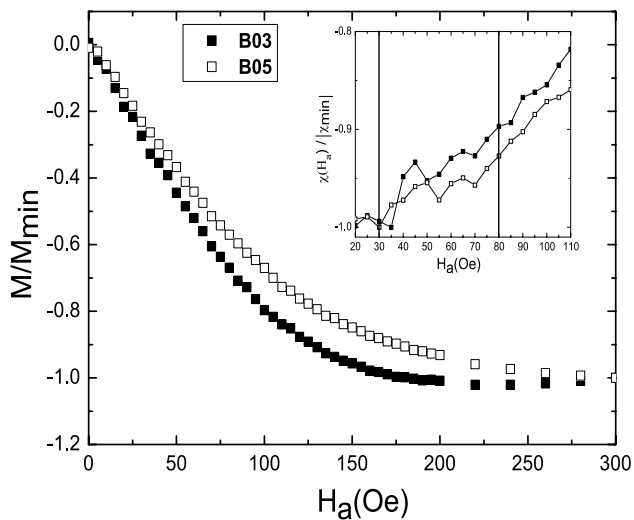


Fig. 3 Magnetization as a function of applied magnetic field of the powder samples B03 and B05. The inset shows the dependence of the normalized susceptibility $\chi/|\chi_{min}|$ as a function of applied magnetic field in the interval $20 < H_a < 110$ Oe of both powder samples. Vertical lines divide the inset in three regions that correspond to the magnetic flux penetration into the Josephson junctions, intragranular planar defects and crystallites, respectively, for increasing magnetic field

the alumina percentage provokes a reduction in the powders grain's size. The subscripts a and c represent the dimensions of the crystallites for the a – b plane and the c direction, respectively, as displayed in Table 1. Also, the ratio $L_a/L_c \sim (10 - 40)$. All these results agree with those reported in Refs. [10, 20, 25]

3.2 $M(H_a)$ curves

In Fig. 3 the normalized magnetization curves, $M(H_a)/M_{min}$, for the two powder samples are shown. These curves exhibit a quasi-linear behaviour in the interval $0 < H_a < 80$ Oe, which is related with the Meissner state of the grains of the powder samples. Both curves display also a Bean-like behaviour [26] in the whole range of applied magnetic field $0 < H_a < 300$ Oe. However, the sample B03 exhibits lower values in whole the range of applied magnetic field, probably related with the different percentage of doping.

The normalized susceptibility curves, $\chi(H_a)/|\chi_{min}|$, shown in the inset of Fig. 3 have been reported before for other types of Bi-2223 samples [10, 12]. The division of the inset in three parts corresponds to the penetration of the magnetic flux into the Josephson junctions, planar defects and crystallites (regions of the grains free of defects), respectively, for increasing H_a values. The explanation to the stepped behaviour of them, which mainly appears in the $30 < H_a < 80$ Oe interval, is based on the penetration of the magnetic flux into the planar defects of the Bi-2223 grains [10, 12]. Thus, the doping with small percentages of α - Al_2O_3 NPs does not modify essentially such behaviour, which is intrinsic of the Bi-2223 phase due to its complex granular structure. However, the doping acts to raise some features of these as shown in Fig. 3. Notice that in both types of curves the B03 sample shows a more pronounced variation with the applied magnetic field.

3.3 Critical current density and flux-trapping curves

The improvement of the critical current density, J_c , and its behaviour under an applied magnetic field, $J_c(H_a)$, can be achieved by introducing efficient pinning centers [16–19] in these materials, but the size of NPs, which are used with that purpose, cannot be arbitrary. When the pinning center is larger than the coherence length, ξ , but smaller than penetration depth, λ , the J_c will increase [27, 28]. Thus, a strong interaction between magnetic flux line network and the (Bi,Pb)-2223 matrix can be expected if $\xi < L < \lambda$, where L is the NPs size [28]. However, it has been suggested that the optimum size for flux pinning centers should be comparable to λ rather than ξ . For (Bi,Pb)-2223, ξ is 2.9 nm and λ is 60–1000 nm [28]. Here, we are using α - Al_2O_3 NPs of ~ 40 nm similar to those used in Ref. [17].

Figure 4 shows the current density versus voltage curves of the B03 and B05 samples. From these curves the critical current densities at zero applied magnetic field and 77 K of the samples resulted to be 163.0 and 74.0 A/cm², respectively, by using the criterion of 1 μV . Similarly to what happens with the magnetic properties, the transport properties of these two samples are different due to the percentage of α - Al_2O_3 NPs used for their elaboration. The critical current of the B03 sample is more than twice the value of this magnitude for the B05 sample. The over-doped sample ($x \geq 0.5$ wt%) are associated with the presence of small areas of α - Al_2O_3 NPs agglomerations distributed between (Bi,Pb)-2223 grains [17]. For that reason, the B05 sample has poorer superconducting transport properties than that doped with 0.3 wt% B03. Thus, these two types of samples were selected because they exhibit the best (B03) and worst (B05) electric transport properties in our sample set, respectively.

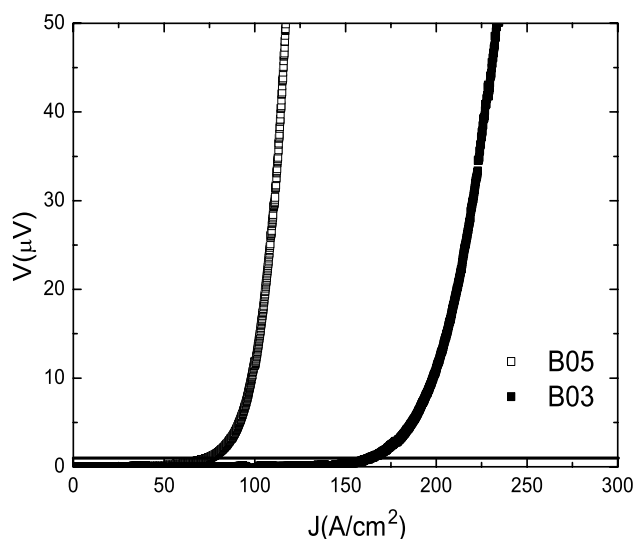


Fig. 4 Critical current density of B03 and B05 samples at zero applied magnetic field and 77 K. The straight line parallel to the J axis represents the criterion of $1 \mu\text{V}$

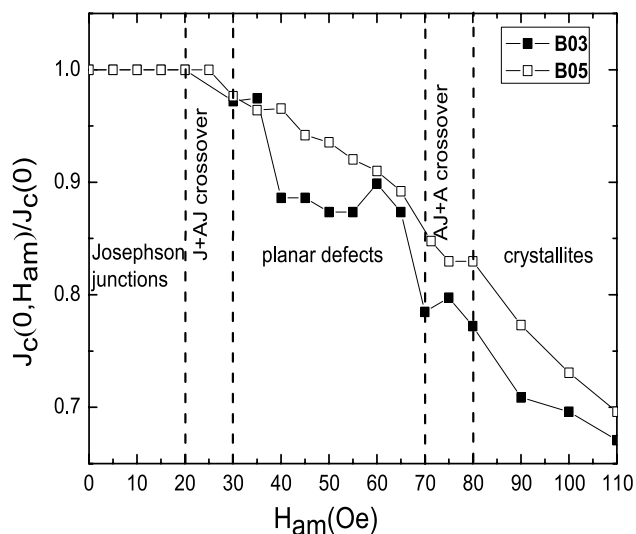


Fig. 5 Normalized critical current density as a function of H_{am} for the B03 and B05 samples. Discontinuous lines show the different regions delimited in the inset of Fig. 3. Here, the crossovers of Josephson (J)–AJ vortices and AJ–A vortices are also shown according to the results reported elsewhere [12]

In Fig. 5 the normalized critical current density as a function of H_{am} for both pellet samples are shown. A combined analysis of

Figures 3 and 5 suggests that the penetration and trapping processes in powder and pellet samples, are also closely related in these samples, similar to the experiment already published for our group [10]. Another important feature to be considered here is that the $J_c(0, H_{am})$ curves of the two samples are also different. The effect of the trapped flux

on the critical current density is more pronounced in B03 sample. The $\alpha\text{-Al}_2\text{O}_3$ NPs in the superconducting matrix can modify appreciably the magnetic flux trapping effects in the B03 sample in comparison with previous results in other types of samples [10, 25]. However, an subsequent increase of the percentage of $\alpha\text{-Al}_2\text{O}_3$ NPs in the total mass of the samples may re-establish the flux trapping properties similar to that of samples without doping. Analogous results have been reported elsewhere [17] in the case of the curves of resistivity as a function of temperature. Finally, the plot of Fig. 5 have been divided in three regions that represent the penetration and trapping of the magnetic flux into the weak links, planar defects and crystallites (regions free of defects), respectively, in similar way as shown in the inset of Fig. 3. In addition, the crossover of Josephson (J)–AJ vortices and AJ–A vortices are also shown according to the results discussed elsewhere [12].

3.4 Voltage relaxation

In previous subsections we have shown that the Bi-2223 ceramic samples doped with $\alpha\text{-Al}_2\text{O}_3$ NPs have a similar behaviour than those exhibit by Cu, Ca enriched samples [10] or non-doped samples compacted at different pressures [25]. Thus, the penetration of the magnetic flux into planar defects for applied magnetic fields lower than 80 Oe seems to be a quite general behaviour in Bi-2223 superconductors. Nevertheless, the magnetic and transport properties of the two samples are modified quantitatively in an appreciable way when the doping with $\alpha\text{-Al}_2\text{O}_3$ NPs is altered. This is an important issue for our purpose, since we have interest in the study of the voltage relaxation in samples with certain amount of trapped flux, which in turn, exhibit different transport and magnetic properties. The main role of the doping with $\alpha\text{-Al}_2\text{O}_3$ NPs is the variation of the pinning energy of the samples. Consequently, a variation in the voltage-relaxation curves should be observed.

Let us start analysing Fig. 6 taking into consideration the results shown in Fig. 4. We focus our attention on relaxation times lower than 50 s, just at the very beginning of the relaxation process corresponding to the B05 sample. In the curve obtained for a maximum applied magnetic field of 30 Oe and excitation current, $I_e = 1.1I_c = 0.815$ A, where I_c is the critical current of the sample, the initial voltage is $2.16 \mu\text{V}$. However, the voltage obtained in the current density versus voltage curve is $1.9 \mu\text{V}$, so the difference is less than of $0.2 \mu\text{V}$. On the other hand, when the maximum applied magnetic field is increased to 50 Oe, the voltage in the relaxation curve is two times the value without the effects of the trapped flux. Thus, this difference is more pronounced for 60 and 70 Oe. The increment of the voltage has two main causes: (a) the dissipation due to the displacement of the AJ vortices in the network

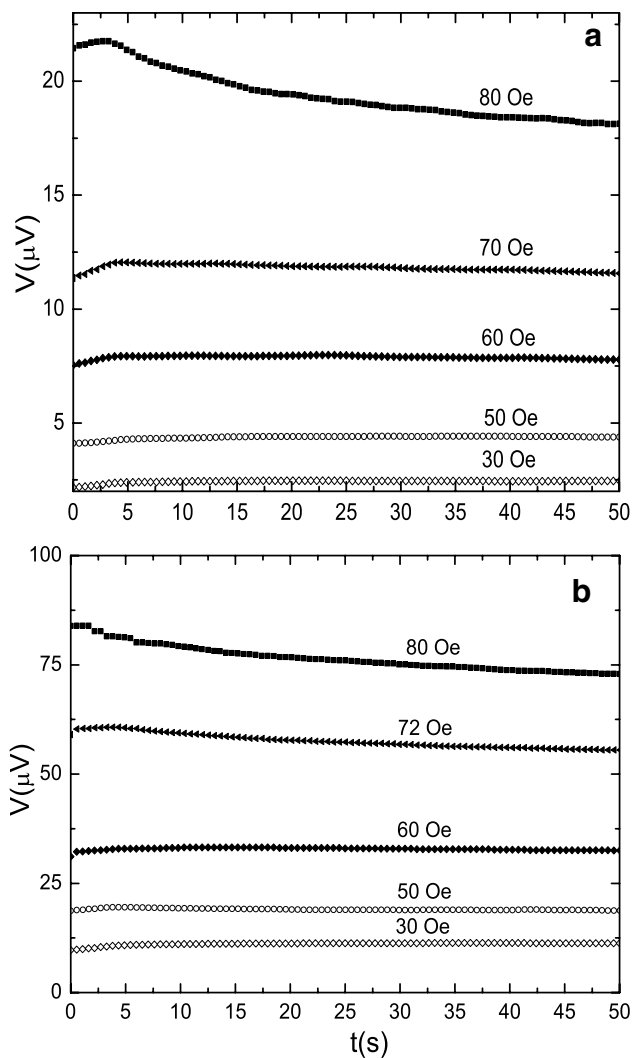


Fig. 6 Voltage relaxation with remnant magnetic flux of the B05 sample at zero applied magnetic field and 77 K. **a** $I_e = 1.1I_c$ and **b** $I_e = 1.3I_c$

of intragranular planar defects, (b) the reduction of the transport capability of the Josephson junctions provoked by the intergranular magnetic field, GM_{pd} . Here, G is an effective demagnetization factor and M_{pd} the intragranular magnetization as consequence of the AJ vortices trapped inside the planar defects. In the studied range of time, for maximum applied magnetic fields inside the interval $30 < H_{am} < 70$ Oe, the behaviour of the curves is the following. First, the voltage increases lightly during the first 5 s and then a almost constant value is established. This behaviour can be explained assuming that the intragranular magnetic flux is confined to the planar defects and therefore the main causes of the dissipation are quasi-stationary. It means that even when the AJ vortices are moving throughout the material, the mean value of M_{pd} is time-independent or its variation can be neglected.

On the other hand, when the applied magnetic field reaches 80 Oe, an appreciable modification in the $V(t)$ curve is observed. The curve reaches a maximum at the first 5 s of the relaxation process and then decrease appreciably. This behaviour is in perfect agreement with the penetration of the magnetic flux inside the crystallites and the emergence of the A vortices. These generate a new component of the intragranular magnetization which is time-dependent because the A vortices are not confined to a small area as the AJ ones. Also, the maximum in the curve may be explained by assuming the emergence of two contrary tendencies. During the first seconds of applying the excitation current the $V(t)$ increases until reaching the speed limit of the AJ vortices in the planar defects network, but at the same time the intragranular magnetization and consequently the intergranular magnetic fields that affect the Josephson junctions starts to decrease due to the modification of the Bean profiles [26] because of the intragranular flux creep [15]. Moreover, the penetration of the magnetic flux into the crystallites relieves the congestion of the magnetic flux inside the planar defects and consequently the voltage generated in the intragranular planar defects decreases. Thus, these contrary tendencies that affect the $V(t)$ curve give place to the observed maximum in the $V(t)$ curve for $H_{am} = 80$ Oe.

In panel (b) of Fig. 6 the results for a higher excitation current, $I_e = 1.3I_c = 0.963$ A. The behaviour is similar to that displayed in the panel (a), but two main differences are observed. First, the maximum in the $V(t)$ curve corresponding to a maximum applied magnetic field of 80 Oe is essentially negligible. The increase of the $V(t)$ dependence at the first 5 s of the relaxation process, for maximum applied magnetic fields lower than 80 Oe, are much less appreciable than in the panel (a). This is an expected result in the framework of our model. When the excitation current increases, the number of Josephson junctions that can sense the effect of the remnant magnetic flux on the voltage is reduced. Nevertheless, a behaviour change at a maximum applied magnetic field of 80 Oe continue to be observed. For example, the voltage drop rate increases appreciably for the curve obtained at 80 Oe as compared with the remaining ones.

Figure 7 shows similar results than those displayed in panel (a) of Fig. 6 for B03 sample. One issue to be highlighted here is that we are dealing with a sample with higher critical current. Thus, once the critical current is surpassed the obtained voltage may be also higher. On the other hand, the B03 sample exhibits similar behaviour than the B05 sample. However, the B03 sample reaches the equilibrium voltage later than the B05 sample. This difference should be related with the better transport properties of the B03 sample.

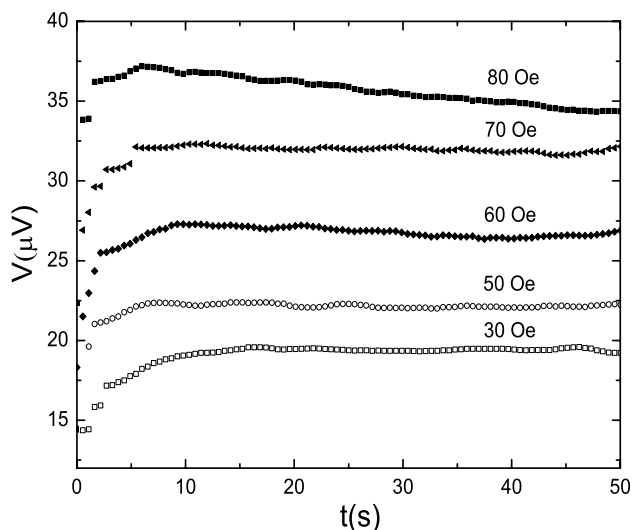


Fig. 7 Voltage relaxation with remnant magnetic flux of the B03 sample at zero applied magnetic field and 77 K. $I_c = 1.1I_c$

To quantify the differences between the behaviours of the both samples let us compare some parameters that can be extracted from Figs. 6a and 7.

The times to reach the equilibrium voltage measured from the curves with $H_{am} = 60$ Oe are 9.23 and 4.35 s for B03 and B05 samples, respectively. Consequently, the peaks in the curves obtained for $H_{am} = 80$ Oe are at 6.0 and 2.7 s, respectively. Notice that the higher values correspond to the B03 sample.

On the other hand, the voltage drop rates calculated by the formula, $\Delta V/V_m$, where $\Delta V = V(50) - V_m$ and V_m is the maximum value of the voltage, are 7.5 and 16.7%, for the B03 and B05 samples, respectively. The data has been extracted from the curves obtained at 80 Oe. However, if these calculations are performed for the curves obtained at 70 Oe of both samples the results are 1.3 and 3.9%, respectively. In addition to that, similar calculations from the curves obtained with $H_{am} = 60$ Oe are approximately 1.8% for both samples. Thus, the penetration of the magnetic flux inside the crystallites results in an appreciable increase of the voltage drop rate for both samples studied in this work. Also the values of the voltage drop rate for the B03 sample are lower than those obtained for the B05 sample. It is related with a better vortex-pinning in the B03 sample than in the B05 sample.

The increase of the excitation current results in a decrease of the voltage drop rate as can be obtained for the B05 sample from Fig. 6. The value of the voltage drop rate for this sample measured with $H_{am} = 80$ Oe and excitation current $1.3I_c$ is 13.2. This value is lower than that obtained for an excitation current $1.1I_c$ in the same sample, but it is still close to be almost two times higher than the value that correspond to the B03 sample for an excitation current of $1.1I_c$.

4 Conclusions

Starting from transport and magnetic measurements, we have shown that Bi-2223 samples doped with α - Al_2O_3 NPs in 0.3 and 0.5% exhibit similar behaviour than those doped with Ca and Cu and non-doped samples [10, 25]. The penetration of the magnetic flux into the planar defects occurs for applied magnetic fields higher than 30 Oe at 77 K, but the crystallites are penetrated at 80 Oe approximately.

We also have revealed some features of the $V(t)$ curves for different maximum applied magnetic fields which characterize the penetration of the magnetic flux within the crystallites and consequently the emergence of the Abrikosov vortices throughout the material. It allows determining the limit between the penetration of the magnetic flux into the planar defects and its penetration into the crystallites. These results can be used as a new method to determine the lower critical field of both, planar defects and crystallites.

The differences observed between the B03 and B05 samples regarding the magnetic and transport measurements have their fingerprint also in $V(t)$ curves. The B03 sample with higher critical current density and more pronounced magnetic flux trapping also shows a larger time interval to reach the equilibrium voltage for applied magnetic field lower than the lower critical field of the crystallites. Moreover, the voltage drop rate when $H_{am} = 80$ Oe is appreciably higher for the B05 sample, which reflects its lower vortex-pinning.

Acknowledgements This work was partially supported by CAPES/MES-CUBA, Project 104/10 and the Belgian Department for Development Cooperation through the Flemish Interuniversity Council University Cooperation for Development (VLIR-UOS) in the framework of an Institutional University Cooperation Programme with Universidad de Oriente, Santiago de Cuba, Cuba. The authors thank to professors E. Martínez-Guerra and F. Solís-Pomar from Centro Investigación en Materiales Avanzados S. C., Unidad Monterrey-PIIT, Apodaca, Nuevo León 66600, México and Centro de Investigación en Ciencias Físico-Matemáticas, FCFM, UANL, Monterrey, Nuevo León, México, respectively. Their help was very important to obtain the SEM micrographs presented in this work. R.F.J. acknowledges support from Brazils agencies FAPESP (Grants Nos. 2013/07296-2, and 2014/19245-6) and CNPq (Grants Nos. 444712/2014-3 and 306006/2015-4).

References

1. H. Kitaguchi, O. Ozaki, T. Miyazaki, N. Ayai, K. Sato, S. Urayama, H. Fukuyama, IEEE Trans. Appl. Supercond. **20**, 710 (2010)
2. Y. Koshiba, S. Yuan, N. Maki, M. Izumi, K. Umemoto, K. Aizawa, Y. Kimura, M. Yokoyama, IEEE Trans. Appl. Supercond. **21**, 1127 (2011)
3. A. Matsumoto, H. Kitaguchi, Supercond. Sci. Technol. **27**, 015002 (2014)
4. F. Feng, T.M. Qu, C. Gu, Y. Xin, W.Z. Gong, W. Wu, Z. Han, Physica C **471**, 293 (2011)

5. M. Noe, M. Steurer, *Supercond. Sci. Technol.* **20**, R15 (2007)
6. H. Hong, Z. Cao, J. Zhang, X. Hu, J. Wang, X. Niu, B. Tian, Y. Wang, W. Gong, Y. Xin, *IEEE Trans. Appl. Supercond.* **19**, 1851 (2009)
7. W.M. Woch, M. Chrobak, M. Kowalik, R. Zalecki, M. Giebul-towski, J. Niewolski, L. Gondek, *J. Alloys Compd.* **692**, 359 (2017)
8. M. Hernández-Wolpez, E. Martínez-Guerra, R.F. Jardim, P. Muné, *Rev. Mex. Fís.* **62**, 515 (2016)
9. F. Nakao, K. Osamura, *Supercond. Sci. Technol.* **18**, 513 (2005)
10. M. Hernández-Wolpez, A. Cruz-García, O. Vázquez-Robaina, R.F. Jardim, P. Muné, *Physica C* **525–526**, 84 (2016)
11. A. Gurevich, *Phys. Rev. B* **46**, R3187 (1992)
12. M. Hernández-Wolpez, A. Cruz-García, R.F. Jardim, P. Muné, *J. Mater. Sci: Mater. Electron.* **28**, 15246 (2017)
13. I. Matsubara, R. Funahashi, K. Ueno, H. Yamashita, T. Kawai, *Physica C* **256**, 33 (1996)
14. R. Job, M. Rosenberg, *Physica C* **172**, 391 (1991)
15. E. Altshuler, J.L. González, *Physica C* **200**, 195 (1992)
16. M. Annabi, A.M. Chirgui, F. Ben Azzouz, M. Zouaoui, M. Ben Salem, *Physica C* **405**, 25 (2004)
17. A. Ghattas, M. Annabi, M. Zouaoui, F. Ben Azzouz, M. Ben Salem, *Physica C* **468**, 31 (2008)
18. A.I. Abou-Aly, S.A. Mahmoud, R. Awad, M.M.E. Barakat, *J. Supercond. Nov. Magn.* **23**, 1575 (2010)
19. D. Yazici, M. Erdem, B. Ozcelik, *J. Supercond. Nov. Magn.* **25**, 725 (2012)
20. P. Muné, E. Govea-Alcaide, R.F. Jardim, *Physica C* **384**, 491 (2003)
21. E. Altshuler, S. García, J. Barroso, *Physica C* **177**, 61 (1991)
22. M.Y. Li, Z. Han, *Supercond. Sci. Technol.* **20**, 843 (2007)
23. M. Pakdil, E. Bekiroglu, M. Oz, N.K. Saritekin, G. Yildirim, *J. Alloys Compd.* **673**, 205 (2016)
24. A.I. Abou-Aly, M.M.H. Abdel Gawad, R. Awad, I. G-Eldeen, *J. Supercond. Nov. Magn.* **24**, 2077 (2011)
25. E. Govea-Alcaide, R.F. Jardim, P. Muné, *Physica C* **423**, 152 (2005)
26. C.P. Bean, *Rev. Mod. Phys.* **36**, 31 (1964)
27. U. Al Khawaja, M. Benhraouda, I.M. Obaidat, S. Alneaimi, *Physica C* **442**, 1 (2006)
28. Nabil A.A. Yahya, R. Abd-Shukor, *Int. J. Electrochem. Sci.* **11**, 3633 (2016)